THE JOURNAL OF BIOLOGICAL CHEMISTRY VOL. 287, NO. 14, pp. 11338–11350, March 30, 2012

Kinetics of α-Globin Binding to α-Hemoglobin Stabilizing Protein (AHSP) Indicate Preferential Stabilization of Hemichrome Folding Intermediate*

Received for publication, October 12, 2011, and in revised form, January 30, 2012 Published, JBC Papers in Press, February 1, 2012, DOI 10.1074/jbc.M111.313247

Todd L. Mollan[‡], Eugene Khandros[§¶], Mitchell J. Weiss[§¶], and John S. Olson[‡1]

From the [‡]Department of Biochemistry and Cell Biology, Rice University, Houston, Texas 77251, [§]Cell and Molecular Biology Group, University of Pennsylvania, Philadelphia, Pennsylvania 19104, and [¶]Division of Hematology, The Children's Hospital of Philadelphia, Philadelphia, Pennsylvania 19104

Background: α-Hemoglobin stabilizing protein (AHSP) facilitates hemoglobin production.
Results: AHSP preferentially binds to ferric *versus* ferrous α subunits and induces reversible structural alterations within seconds of binding.
Conclusion: AHSP exerts its effects by stabilizing a ferric α folding intermediate and inhibiting its participation in hemoglobin assembly.
Significance: AHSP is a molecular chaperone for ferric α-globin.

Human α-hemoglobin stabilizing protein (AHSP) is a conserved mammalian erythroid protein that facilitates the production of Hemoglobin A by stabilizing free α-globin. AHSP rapidly binds to ferrous α with association (k'_{AHSP}) and dissociation (k_{AHSP}) rate constants of ≈10 μM^{-1} s^{-1} and 0.2 s^{-1}, respectively, at pH 7.4 at 22 °C. A small slow phase was observed when AHSP binds to excess ferrous αCO. This slow phase appears to be due to cis to trans prolyl isomerization of the Asp^{29}-Pro^{30} peptide bond in wild-type AHSP because it was absent when αCO was mixed with P30A and P30W AHSP, which are fixed in the trans conformation. This slow phase was also absent when met(Fe^{3+})-α reacted with wild-type AHSP, suggesting that met-α is capable of rapidly binding to either Pro^{30} conformer. Both wild-type and Pro^{30}-substituted AHSPs drive the formation of a met-α hemichrome conformation following binding to either met- or oxy(Fe^{2+})-α. The dissociation rate of the met-αAHSP complex (k_{AHSP} ≈ 0.002 s^{-1}) is ~100-fold slower than that for ferrous αAHSP complexes, resulting in a much higher affinity of AHSP for met-α. Thus, *in vivo*, AHSP acts as a molecular chaperone by rapidly binding and stabilizing met-α hemichrome folding intermediates. The low rate of met-α dissociation also allows AHSP to have a quality control function by kinetically trapping ferric α and preventing its incorporation into less stable mixed valence Hemoglobin A tetramers. Reduction of AHSP-bound met-α allows more rapid release to β subunits to form stable fully, reduced hemoglobin dimers and tetramers.

Hemoglobin A (HbA)[2] is a highly conserved dioxygen transport protein present in red cells of all mature, healthy vertebrates (1). Because of its functional importance, abundance, and experimental tractability, this protein is a model system for a wide variety of biochemical and medical studies (1, 2). One important research aim is to better understand how HbA is synthesized and maintained *in vivo* because dysregulation of this process often results in serious anemias, including structural hemoglobinopathies and thalassemia syndromes (3, 4).

HbA production includes α and β gene transcription and translation, subunit folding, heme binding to the aposubunits, redox regulation, and subunit assembly into tetramers (5–9). The end product, HbA, is a heterotetramer containing two pairs of non-covalently associated α and β subunits, each bearing one iron-containing protoporphyrin IX prosthetic group (heme (Fe^{2+}) or hemin/hematin (Fe^{3+})) (1, 10).

α-Hemoglobin stabilizing protein (AHSP) is an erythroid protein that rapidly and reversibly binds to monomeric forms of apo- and holo-α but not β, αβ dimers, or tetrameric HbA (11, 12). AHSP binds α in a 1:1 stoichiometry using a surface that excludes β (12–15), and it has been shown to induce numerous structural changes following binding (14–18). Current evidence suggests that AHSP is a molecular chaperone for HbA production (for reviews, see Refs. 19–21). However, questions remain regarding its role in α prosthetic group acquisition, oxidation state maintenance, subunit folding, and stabilization prior to incorporation into HbA.

In this work, we used optical absorbance and fluorescence emission spectroscopy in stopped-flow rapid mixing experiments to measure the rates of α binding to and release from AHSP. In agreement with work done by Gell *et al.* (16), we report that the affinity of AHSP is dependent on α oxidation state and for the first time show that the rate of met-α dissociation from AHSP is dramatically slower than that for reduced α dissociation. Experiments with clinically significant and rationally selected AHSP and α mutants revealed the functional

* This work was supported, in whole or in part, by National Institutes of Health Grants HL47020 (to J. S. O.), GM35649 (to J. S. O.), DK61692 (to M. J. W.), HL087427 (to M. J. W.), and GM008362 (to T. L. M.). This work was also supported by Welch Grant C-0612 (to J. S. O.).

[1] To whom correspondence should be addressed: Dept. of Biochemistry and Cell Biology, Rice University, P. O. Box 1892, MS-140, Houston, TX 77251. Tel.: 713-348-4762; Fax: 713-348-5154; E-mail: olson@rice.edu.

[2] The abbreviations used are: HbA, Hemoglobin A; α^{WT}, wild-type α subunits; AHSP, α-hemoglobin stabilizing protein; $AHSP^{WT}$, recombinant human wild-type AHSP with an N-terminal Gly-Ser dipeptide; β^{WT}, wild-type β subunits; Hb, hemoglobin; heme, ferroprotoporphyrin IX; hemin, ferriprotoporphyrin IX; met, ferric oxidation state.

importance of the loop separating α-helices 1 and 2 of AHSP. Collectively, this work suggests that AHSP stabilizes α *in vivo* by preferentially binding an oxidized α hemichrome folding intermediate and temporarily impairing α assembly into HbA until reduction to the ferrous state has occurred.

EXPERIMENTAL PROCEDURES

Recombinant Human AHSP Expression and Purification—AHSP protein was obtained from pGEX-2T (GE Healthcare) with the full-length human *AHSP* gene inserted downstream of the *Schistosoma japonicum* glutathione *S*-transferase gene (pGEX-2T-AHSP) (GenBank™ accession number NM_016633.2) (11, 12). AHSP mutants were generated using a QuikChange II site-directed mutagenesis kit (Agilent Technologies, Inc., Santa Clara, CA) in accordance with manufacturer's instructions and the following PCR primers: $AHSP^{P30A}$, 5′-CTG AAT CAG CAG GTC TTC AAT GAT GCG CTC GTC TCT GAA GAA GAC-3′ and 5′-GTC TTC TTC AGA GAC GAG CGC ATC ATT GAA GAC CTG CTG ATT CAG-3′; $AHSP^{P30W}$, 5′-ATC AGC AGG TCT TCA ATG ATT GGC TCG TCT CTG AAG AAG ACA TG-3′ and 5′-CAT GTC TTC TTC AGA GAC GAG CCA ATC ATT GAA GAC CTG CTG AT-3′; $AHSP^{Q25K}$, 5′-CAG CGT TCT GCT GAA TCA GAA GGT CTT CAA TGA TCC TCT C-3′ and 5′-GAG AGG ATC ATT GAA GAC CTT CTG ATT CAG CAG AAC GC TG-3′; $AHSP^{D29R}$, 5′-AAT CAG CAG GTC TTC AAT CGT CCT CTC GTC TCT GAA GAA G-3′ and 5′-CTT CTT CAG AGA CGA GAG GAC GAT TGA AGA CCT GCT GAT T-3′. Primers were obtained from Integrated DNA Technologies, Inc. (Coralville, Iowa).

AHSP was expressed as a GST fusion protein using *Escherichia coli* BL21 cells (EMD Biosciences, Inc., San Diego, CA; Novagen brand) using methods developed previously (11, 12). The soluble GST-AHSP present in the supernatant was captured using ~25 ml of glutathione-Sepharose FF medium and an ÄKTA FPLC system (GE Healthcare). During this process, PBS was used as a binding and wash buffer, and 50 mM Tris-HCl, 10 mM reduced glutathione, pH 8.0 at 25 °C was used as an elution buffer. GST was cleaved from AHSP using 500 units of thrombin obtained from GE Healthcare. Reduced glutathione, free GST, thrombin, uncleaved AHSP, and other contaminants were then removed by size exclusion chromatography using a preparative grade Superdex 75 HiLOAD prepacked column (GE Healthcare). Yields of GST-free AHSP were ~10 mg/liter of bacterial culture. The AHSP produced using this method contains an extra N-terminal Gly-Ser dipeptide appendage due to the thrombin cleavage site (12).

Recombinant Hb Turriff Production—Hb Turriff was produced using an expression system developed previously (22) and a mutated version of the pHE2 plasmid provided by C. Ho and T-J. Shen (Carnegie Mellon University, Pittsburgh, PA). HbA bearing α^{K99E} was produced by site-directed mutagenesis and the following mutagenic primers: 5′-CCG GTT AAC TTC GAA CTG CTG TCT CAC TGC C-3′ and 5′-GGC AGT GAG ACA GCA GTT CGA AGT TAA CCG G-3′. Recombinant Hb Turriff was expressed and purified using the methods described by Birukou *et al.* (23).

Native Human HbA Purification and Chain Isolation—HbA was purified from units of human blood obtained from the Gulf Coast Regional Blood Center (Houston, TX) using established methods (24). Separated α and β chains were isolated using established methods (25, 26) that were modified as follows. Incubation of CO-liganded HbA with 4-(hydroxymercuri)benzoic acid was limited to ~4 h at 4 °C instead of overnight. Following this incubation, samples were rapidly buffer-exchanged into 10 mM Tris-HCl, pH 8.0 at 4 °C using a column containing 200 ml of Sephadex G-25 medium (Sigma-Aldrich). Samples were then applied to another column containing 100 ml of diethylaminoethyl cellulose medium that had been equilibrated with the same buffer (DE52 medium, Whatman). This column retains β and tetrameric HbA while allowing α to flow through. HbA was then eluted with 20 mM Tris-HCl, pH 7.4 at 4 °C, and β was eluted using 100 mM Tris-HCl, pH 7.0 at 4 °C. Rather than regenerating sulfhydryl groups using the methods of Geraci *et al.* (25), a final concentration of 5 ml/liter β-mercaptoethanol was added to each sample on ice after which the samples were immediately exchanged into 10 mM Tris-HCl, pH 8.0 at 4 °C using a column containing 200 ml of Sephadex G-25 medium. This entire process was done in less than 8 h, and all work was done in a room maintained at 4 °C. Regeneration of sulfhydryl groups was assayed by Boyer titration (27). Chain isolations were done in 4-ml batches of 50 mg/ml HbA.

Protein Identity, Purity, and Stability Verification—Plasmid DNA was isolated from each AHSP expression and sent for sequencing to Lone Star Laboratories, Inc. (Houston, TX) using manufacturer-specified sequencing primers to verify the absence of any unwanted mutations. These primers were 5′-GGG CTG GCA AGC CAC GTT TGG TG-3′ and 5′-CCG GGA GCT GCA TGT GTC AGA GG-3′. SDS-PAGE gels stained with Coomassie Blue were used to confirm protein expression; GST cleavage; and GST, thrombin, and contaminant removal. MALDI-TOF spectrometry performed at Rice University (Houston, TX) confirmed the identity and purity of AHSP. HbA, α, and β purities and reassembly efficiency were verified by cellulose acetate electrophoresis (Helena Laboratories Corp., Beaumont, TX). Absorbance spectra and ligand binding kinetics were also verified to ensure that the samples retained normal function following purification and isolation (28). Heme protein concentrations were determined using extinction coefficients reported previously (29, 30). With the exception of $AHSP^{P30W}$, AHSP concentrations were determined by optical absorbance at 280 nm using the extinction coefficient 11,460 M^{-1} cm^{-1}, which was calculated using the ExPASy Proteomics Server ProtParam Tool. The extinction coefficient used for $AHSP^{P30W}$ was 16,960 M^{-1} cm^{-1}, which was calculated in the same manner.

Instrumentation and Materials—Manual mixing spectrophotometry was done in either a Cary 50Bio (Varian, Inc., Palo Alto, CA) or a UV2401PC spectrophotometer (Shimadzu, Inc., Columbia, MD) using cuvettes purchased from Starna Cells (Atascadero, CA). Stopped-flow spectrophotometry was done using either a modified Durrum Model D-110 (Palo Alto, CA) or an Applied Photophysics PiStar kinetic circular dichroism stopped-flow spectrophotometer (Leatherhead, Surrey, UK). Unless otherwise indicated, all stopped-flow fluorescence

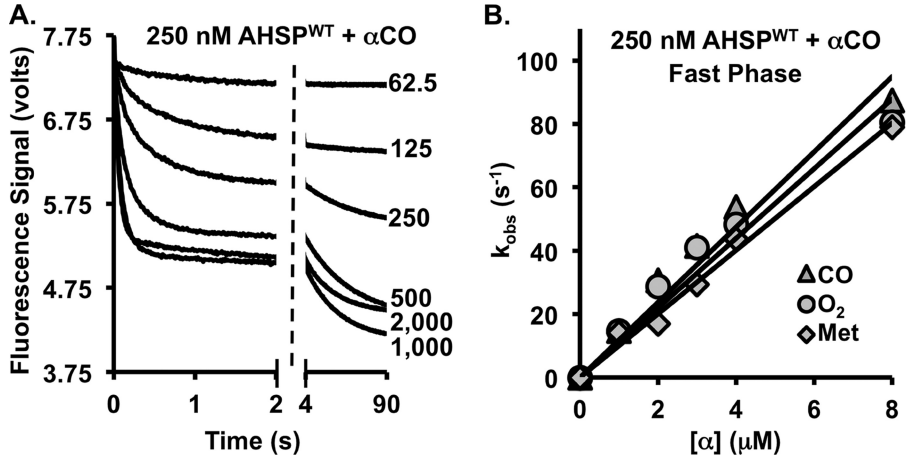

FIGURE 1. **Time courses and association rate constants for αCO^{WT} binding to $AHSP^{WT}$.** *A*, fluorescence signal changes after rapidly mixing αCO^{WT} with $AHSP^{WT}$. *Numbers* in the *right margin* represent the postmixing nanomolar (nM) concentrations of αCO^{WT}. Control reactions designed to account for the potential effects of photobleaching, precipitation, denaturation, and aggregation were performed, and no changes occurred on the time scales shown (data not shown; see Ref. 28). *B*, determination of bimolecular association rate constant for $AHSP^{WT}$ binding to both reduced and oxidized α^{WT} (k'_{AHSP}) under pseudo-first-order conditions. The *lines* represent fits to an expression derived from Reaction 1 with the *y*-intercept fixed to values of k_{AHSP} measured directly by βCO displacement (Table 1 and Fig. 5). Buffers were bubbled with the indicated gases prior to use. To generate ferric α^{WT}, a 5-fold molar excess of potassium ferricyanide was added to $\alpha O_2{}^{WT}$ prior to the experiment, and the samples were stored on ice to inhibit denaturation and precipitation of met-α. All concentration values are postmixing.

experiments were performed using exit and entrance slit widths of 5 nm for the excitation monochromator, an excitation wavelength of 280 nm, and a cutoff filter fitted to the sample housing that allowed the measurement of total sample fluorescence emission above a wavelength of 302 nm. The volume of the cell was 20 μl, and the excitation pathlength of the incident light was 10 mm. The photomultiplier unit was positioned at a 90° angle from the incident light, and the fluorescence cell width was 1 mm (total cell dimensions were $10 \times 2 \times 1$ mm). Shot volumes were between 100 and 200 μl, and mixing was performed using equal volumes of reactant solutions.

Unless otherwise noted, all experiments were performed using 50–150 mM potassium phosphate buffer, pH 7.4 at 22 °C, and all concentrations are given as postmixing. Glass syringes were used whenever possible in the stopped-flow experiments to prevent atmospheric gas contamination (Cadence Science, Lincoln, RI). All buffers, salts, and medium components used for these experiments were obtained from either Sigma-Aldrich or Fisher Scientific. CO and O_2 gases were obtained from Matheson Tri-gas, Inc. (Basking Ridge, NJ).

Data Analysis and Figure Production—Microsoft Excel was used for nonlinear least square data fitting (Microsoft Corp., Redmond, WA) (31). Theoretical data sets calculated from the expressions defined in the text were put into an Excel spreadsheet along with experimentally obtained data, and the sum of the squared residuals were minimized using the Excel Solver tool to obtain visual assessments of plots of the observed and theoretical time courses. Fitting routines in Origin were also used to verify the values obtained from Excel (OriginLab Corp., Northampton, MA). Structure images were created using the PyMOL Molecular Graphics System (Schrödinger, LLC, New York, NY).

RESULTS

Rates of AHSP Binding to Native α—Recombinant human wild-type AHSP ($AHSP^{WT}$) exhibits intrinsic fluorescence from several aromatic side chains (32). Although wild-type human α and β also contain these residues, neither of these subunits exhibit strong intrinsic fluorescence due to highly efficient fluorescence resonance energy transfer to their heme prosthetic groups (33, 34). When α binds to AHSP, this energy transfer quenches the intrinsic fluorescence of AHSP. The key residue in this process is thought to be AHSP Trp^{44} (32), which is solvent-exposed in unbound AHSP and becomes buried when α is bound (14).

Baudin-Creuza *et al.* (32) were the first to report that fluorescence quenching occurs upon formation of a complex between α and AHSP. Their data are consistent with a simple one-step bimolecular association reaction (32).

$$\alpha + \text{AHSP} \underset{k_{AHSP}}{\overset{k'_{AHSP}}{\rightleftharpoons}} \alpha\cdot\text{AHSP}$$

REACTION 1

We confirmed and extended their work using a stopped-flow fluorometer to measure the rates of association (k'_{AHSP}) and dissociation (k_{AHSP}) (19), and our initial kinetic measurements were subsequently confirmed by Brillet *et al.* (35).

As shown in Fig. 1*A*, mixing α^{WT} with $AHSP^{WT}$ resulted in rapid fluorescence quenching on time scales of less than 100 s. The observed time courses for wild-type AHSP are biphasic with a fast phase showing a rate that is linearly dependent on $[\alpha^{WT}]$ and a smaller (20–30%) slow phase showing an observed rate that is concentration-independent and equal to 0.04 ± 0.01 s^{-1} in 100 mM phosphate buffer at pH 7.4 at 22 °C. This slow phase was not present when the concentration of α^{WT} was substantially less than that of $AHSP^{WT}$.

The titration in Fig. 1*A* indicates that the fast phase of the binding reaction corresponds to a bimolecular association event, which is consistent with previous studies of the formation of reduced α·AHSP complexes (11, 12, 14, 19). The associ-

TABLE 1

Rates of α binding to and dissociation from AHSP^{WT}, AHSP^{P30A}, and AHSP^{P30W}

The association (k'_{AHSP}) and dissociation (k_{AHSP}) rate constants were obtained from kinetic data similar to those in Figs. 1, 2, and 5. The equilibrium dissociation constant ($K_{D(AHSP)}$) was calculated from the ratio k_{AHSP}/k'_{AHSP}. The $K_{D(AHSP)}$ values reported by Gell *et al.* (12, 16) are given in parentheses and were determined by isothermal titration calorimetry in 20 mM sodium phosphate buffer at pH 7.0 at 20 °C using 450 mM sucrose in the case of ferric αHb^{WT} to mitigate precipitation. Gell *et al.* (16) did not report a $K_{D(AHSP)}$ for αCO binding to AHSP^{P30W}; the value for this reaction in the last row is for αO_2. The association and dissociation rate constants (k'_{AHSP} and k_{AHSP}, respectively) reported by Brillet *et al.* (35) are shown in brackets and were determined in PBS at 37 °C.

Reaction	k'_{AHSP}	k_{AHSP}	$k'_{\alpha\beta}$	$K_{D(AHSP)}$
	$\mu M^{-1} s^{-1}$	s^{-1}	$\mu M^{-1} s^{-1}$	nM
AHSP^{WT} + α^{WT}CO	10 ± 1.9 [20][a]	0.17 [0.35]	0.26	17 [17] (93)
AHSP^{WT} + $\alpha^{WT}O_2$	11[a]	0.18	0.20	18 (98)
AHSP^{WT} + met-α^{WT}	10	0.0017	1.0	0.17 (4.3)
AHSP^{P30A} + α^{WT}CO	9.2	0.14	0.19	15 (38)
AHSP^{P30A} + met-α^{WT}	11[b]	0.0066[b,c]	0.5[b]	0.60[b]
AHSP^{P30W} + α^{WT}CO	13	0.0072	1.4	0.56 (7.7)
AHSP^{P30W} + met-α^{WT}	17[b]	0.0042[b,c]	0.5[b]	0.24[b]

[a] A slow second phase (~25% amplitude) is observed with a first-order rate equal to 0.04 s^{-1} that is independent of [α] (Fig. 1*A*).

[b] The rate parameters for met-α^{WT} binding and release from AHSP^{P30A} and AHSP^{P30W} were determined from a more limited set of data than those for the other reactions. Binding was estimated from one set of concentrations, and release was measured at one high [β] with the value of $k'_{\alpha\beta}$ fixed to the average value obtained by McGovern *et al.* (39). Time courses for these reactions are provided in Fig. 2 of Khandros *et al.* (36).

[c] The time course for met-α dissociation from AHSP^{P30A} indicated two phases, and fitting to a two-exponential expression gave a fast phase with an amplitude of ~33% and k_{AHSP} of ≈0.04 s^{-1} and a slow phase with an amplitude of ~67% and k_{AHSP} of ≈0.002 s^{-1}. The larger rate is still significantly slower that the rate of dissociation of reduced α from this mutant. The value in the table was calculated from the half-time of the reaction. Similar analyses of the met-α AHSP^{WT} and AHSP^{P30W} dissociation reactions indicate that if any fast phases exist their amplitudes are ≤15% of the total fluorescence changes (see Fig. 2*B* in Khandros *et al.* (36)).

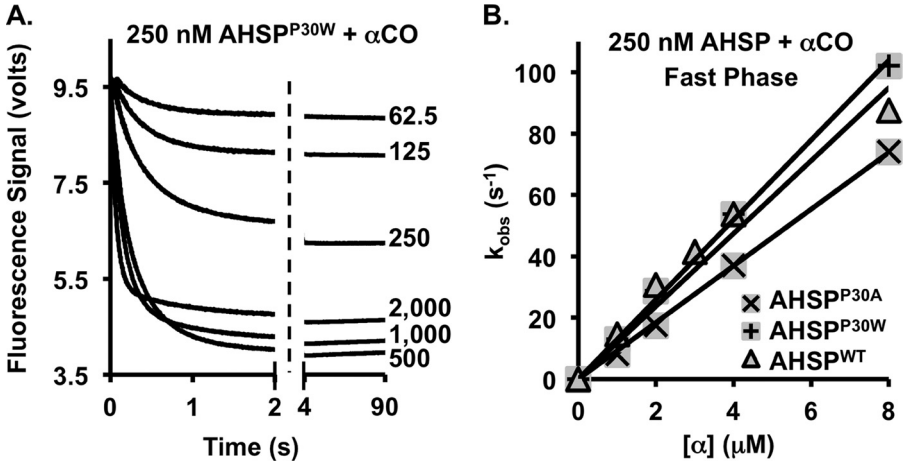

FIGURE 2. **Effects of Pro^{30} mutation of AHSP on α binding.** *A*, time courses for the reaction of α^{WT} with AHSP^{P30W}. The postmixing [α^{WT}] in nM is given *beside* each trace. Experiments with AHSP^{P30A} also showed no detectable slow phase (see Fig. 2A in Khandros *et al.* (36)). The decreases in the fluorescence changes at high micromolar α^{WT} concentrations were the result of light scattering, giving higher background signals. They are consistently observed in all experiments regardless of mutation at [αCO] ≥~1 μM (28). *B*, determination of the bimolecular association rate constant for αCO^{WT} binding to AHSP^{P30A} and AHSP^{P30W} under pseudo-first-order conditions. *Lines* represent fits to Reaction 1 with the *y*-intercept fixed to values of k_{AHSP} measured directly by βCO displacement (Table 1 and Fig. 5).

ation rate constant, k'_{AHSP}, was obtained by plotting the observed rates (k_{obs}) for the fast phase against [α] under pseudo-first-order conditions when α^{WT} was in molar excess (Fig. 1*B*). In this plot, the slope of the line is equal to k'_{AHSP}. Fitting data from three independent experiments gave a k'_{AHSP} value of 10 ± 1.9 $\mu M^{-1} s^{-1}$ for AHSP^{WT} in 50 mM potassium phosphate buffer at pH 7.4 at 22 °C. This bimolecular rate is not altered by oxidation of α^{WT} heme iron to the ferric (met-α) state nor is the rate constant for αO_2 binding appreciably different from that of αCO binding (see Fig. 1*B*, Table 1 in this paper, and Fig. 2*A* in Khandros *et al.* (36)).

Santiveri *et al.* (13) reported that AHSP^{WT} exists in solution as a spontaneously interconverting mixture of two structural conformers due to peptidylprolyl cis-trans isomerization at its Asp^{29}-Pro^{30} peptide bond. We hypothesized that the slow phase shown in Fig. 1*A* is related to this phenomenon. We mutated Pro^{30} to an Ala, which cannot undergo cis-trans isomerization. This P30A mutation was reported previously to eliminate AHSP conformational heterogeneity in favor of a structure that is similar to the trans Asp^{29}-Pro^{30} conformation of AHSP^{WT} (13, 14). We also mutated Pro^{30} to Trp, which had the same effect while conferring greater intrinsic fluorescence (not shown) and altered affinity for α.

When α^{WT} was rapidly mixed with either AHSP^{P30A} or AHSP^{P30W}, no slow phase was detected, and the entire reaction is a simple bimolecular process. Representative time courses for AHSP^{P30W} and plots from these experiments are shown in Fig. 2, *A* and *B*. The amplitudes of the total fluorescence decreases for the P30A mutant are virtually identical to those for the sum of the fast and slow phases for wild-type AHSP (not shown; see Ref. 29). In contrast, the changes for AHSP^{P30W} are roughly twice those for AHSP^{WT} in Fig. 1*A* because of the extra Trp side chain. The observed values of k'_{AHSP} for the AHSP Pro^{30} mutants are similar to those for the fast phase in α binding to AHSP^{WT} (Table 1).

As depicted in Fig. 3, *A* and *B*, structural alignments from two previously published NMR studies indicate that AHSP^{P30A} is more similar to the trans Asp^{29}-Pro^{30} peptide bond conformer

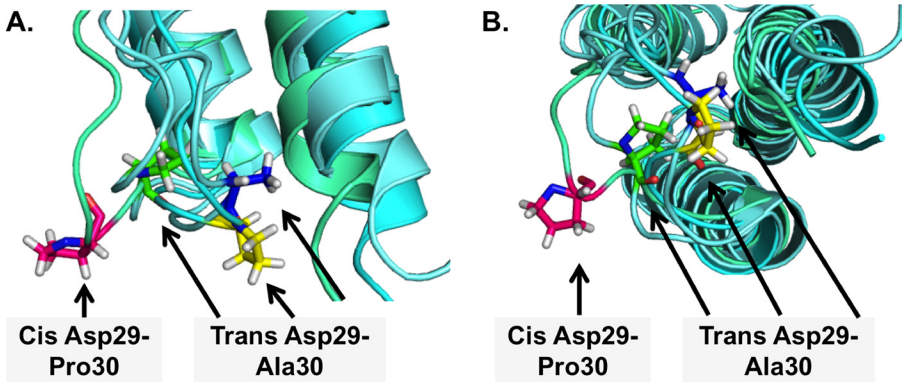

FIGURE 3. **Structural comparison of AHSP^{P30A} with cis and trans Asp^{29}-Pro^{30} peptide bond conformers of AHSP^{WT}.** *A* and *B*, AHSP structures shown as *cyan* and *green ribbons* with residue 30 shown using *variegated sticks*. *Pink stick* structures represent Pro^{30} in the cis peptidylprolyl conformation as it is situated in an NMR solution structure of AHSP (Protein Data Bank code 1W09 (13)). *Blue*, *green*, and *yellow stick* structures depict the trans peptide bond conformation of this residue based on other structural data (Protein Data Bank codes 1W0B (13), 1XZY (14), and 1W0A (13), respectively). Residue 30 in structure 1W0B (*blue*) is an Ala, in 1XZY (*green*) is a Pro, and in 1W0A (*yellow*) is a Pro. Corey-Pauling-Koltun coloring is otherwise used throughout. Notably, x-ray crystal structures for both ferric and ferrous α·AHSP complexes have been reported (14, 15). These structures were both obtained using α^{WT}·AHSP^{P30A} complexes, suggesting that AHSP with a trans Asp^{29}-Pro^{30} peptide bond can accommodate α of either oxidation state. A more recent x-ray structure of a ferric complex bearing AHSP Pro^{30} and a cis Asp^{29}-Pro^{30} peptide bond conformation has also been reported (16). These structural data suggest that ferric α can accommodate either AHSP peptide bond conformation.

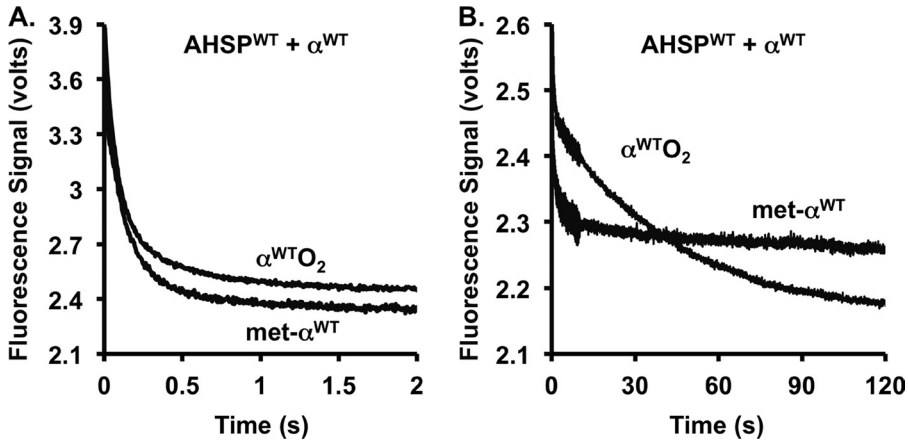

FIGURE 4. **Effects of oxidation on α^{WT} binding to AHSP^{WT}.** *A*, fast phase for the association reaction. *B*, slow phase for the association reaction. The reactions were initiated by mixing 1 μM α^{WT}O$_2$ or met-α^{WT} with 1 μM AHSP^{WT} and monitoring changes in total fluorescence emission signal. The designation "met" is used to refer to the ferric iron or hemin oxidation state. The met-α sample was generated using the same α^{WT}O$_2$ solution by adding a 5-fold excess of ferricyanide to the sample a few minutes prior to the experiment. Note that the *y* axis in *B* is smaller, and the rate of the slow phase for α^{WT}O$_2$ to AHSP^{WT} is approximately the same as that for α^{WT}CO binding shown in Fig. 1*A*.

of AHSP^{WT} than the cis conformer (13, 14). Combined with our kinetic data, these structural data suggest that the fast phase shown in Fig. 1*A* is due to the association of ferrous α^{WT} with the trans Asp^{29}-Pro^{30} AHSP^{WT} conformer. These data also suggest that the slow phase represents a rate-limiting cis-to-trans isomerization of the Asp^{29}-Pro^{30} peptide bond followed by rapid binding.

The reaction of AHSP^{WT} with met-α^{WT} also lacks a slow phase (Fig. 4). The total amplitude changes are similar to those for the AHSP reaction with either αO_2^{WT} and αCO^{WT}, suggesting that met-α can bind to either the cis or trans AHSP^{WT} conformers during bimolecular association perhaps because of greater conformational flexibility.

To investigate further our interpretation of the slow phase, peptidylprolyl isomerases were added to the solutions of AHSP^{WT} prior to mixing with αCO. We tried recombinant cyclophilin-A and FK506-binding protein 4 (Prospec Protein Specialists, East Brunswick, NJ). However, no detectable change in the amplitude or rate of the slow phase was observed after preincubation of AHSP^{WT} with either of these enzymes (data not shown). Either the active sites of these enzymes have specificities that preclude interaction with AHSP^{WT}, or the origin of the slow phase results from some other type of conformational isomerization at the Pro^{30} loop.

Rates of α Dissociation from AHSP Complex—Gel filtration chromatography and electrophoretic mobility shift assays have shown that β subunits are capable of competitively displacing α from AHSP (11, 12, 15). HbA formation occurs during this process because (*a*) α has a much higher affinity for β than for AHSP (12, 37) and (*b*) α cannot simultaneously bind to AHSP and β because both of these interactions involve the same set of interfacial α helices (14, 15). A scheme showing these interactions is given in Fig. 5*A*.

The only species in Fig. 5*A* that exhibits strong intrinsic fluorescence in solution is AHSP when it is not in complex with holo-α (19, 32). When α·AHSP complexes are mixed with β, displacement of α from AHSP increases fluorescence emission

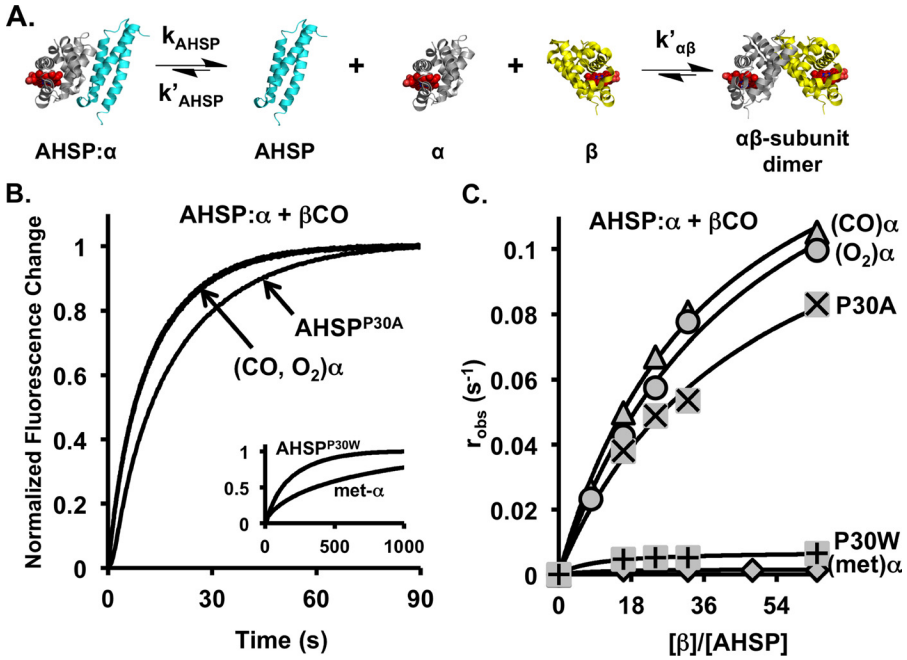

FIGURE 5. **Mechanism, time courses, and rates of displacement of α^{WT} from AHSP complexes by β.** *A*, scheme for the interactions of AHSP, α-, and β-globins. Heme groups are shown as *red balls*, and the color schemes for ribbon structures are as follows: α^{WT}, *gray*; β^{WT}, *yellow*; and AHSP^{WT}, *teal*. Structures were generated using Protein Data Bank codes 1Z8U (AHSP) and 1GZX ($HbAO_2$) (15, 69). *B*, normalized time courses for the displacement of α^{WT} from the AHSP^{WT} complex by β^{WT} showing fluorescence increases. *Inset*, time courses for α^{WT}CO release from AHSP^{P30W} and met-α release from AHSP^{WT} shown on a 10-fold longer time scale. Similar time courses for met-α release from AHSP^{WT} and the Pro^{30} mutants are shown in Fig. 2B of the accompanying paper (36). *C*, plot of the observed replacement rate (r_{obs}) *versus* [βCO]/[AHSP] and theoretical fits to the expression in Equation 1 as described in the text. Because β readily self-associates to form homotetramers (70), an upper limit of 8.0 μM β subunits (postmixing concentration) was used to avoid complications of β tetramer formations based on the equilibrium constant reported by McGovern *et al.* (39), $K_{4,1} = 1.25 \times 10^{-14}$ M^3.

as free AHSP is generated. The rate of this process allows measurement of k_{AHSP} (19, 32, 35).

The observed time courses for the reaction of β with ferrous α·AHSP complexes are monophasic at high concentrations, and the rate of displacement increases with increasing [β]. Representative time courses for a set of displacement reactions are shown in Fig. 5*B*, and a more detailed comparison of time courses for ferric and ferrous α dissociation from wild-type and the Pro^{30} mutants of AHSP is given in Fig. 2B of Khandros *et al.* (36). The amplitudes of the fluorescence increases for α displacement from the various AHSP complexes are slightly smaller in magnitude than the decreases observed in the association experiments (28). The smaller fluorescence increases are mostly likely due to the higher level of background absorbance and light scattering that occur with the addition of excess β. As expected, displacement of α from ASHP^{P30W} showed roughly twice the increase as from AHSP^{WT} due to the presence of a second Trp.

At high AHSP and β concentrations, the amount of free α during the displacement reaction is small throughout the reaction. Under these conditions, the rate of α displacement from AHSP by β is given by the following equation, assuming a steady-state for free α,

$$r_{obs} = \frac{k_{AHSP}k'_{\alpha\beta}[\beta]}{k'_{\alpha\beta}[\beta] + k'_{AHSP}[AHSP]} \quad \text{(Eq. 1)}$$

where k_{AHSP} is the rate constant for dissociation of the α·AHSP complex, k'_{AHSP} is the association rate constant for complex formation, and $k'_{\alpha\beta}$ is the bimolecular rate constant for the association of free Hb subunits to form an αβ dimer (38). By measuring the observed rate of replacement (r_{obs}) at increasing [β], this equation can be used to obtain fitted values for k_{AHSP} and the ratio of k'_{AHSP} to $k'_{\alpha\beta}$ (19). Representative fits to Equation 1 are shown in Fig. 5*C*.

In these studies, low concentrations of α·AHSP complexes were mixed with 5-fold or greater concentrations of β. These concentrations introduce a departure from pseudo-first-order conditions, making Equation 1 approximate because the free concentration of AHSP is increasing from zero during the reaction. To address this, we fixed the free [AHSP] in Equation 1 to 50% of the postmixing total AHSP concentration (0.125 μM). Then r_{obs} values were determined by either fitting the observed time courses to a single exponential expression or computed from the measured half-time ($r_{obs} = \ln 2/t_{1/2}$). This simplified analysis provides fitted values for k_{AHSP} that are identical to those obtained by numerical integration of the rate equations that allow the concentration of AHSP to increase with time (35), and good fits to plots of r_{obs} *versus* [β] were obtained (Fig. 5*C*).

For the fits to Equation 1 shown in Fig. 5*C*, the value of k'_{AHSP} was fixed to the value determined from the bimolecular association reactions shown in Figs. 1*B* and 2*B*, and k_{AHSP} and $k'_{\alpha\beta}$ were allowed to vary. Table 1 summarizes the results of several displacement experiments involving the dissociation of ferric and ferrous α^{WT} from AHSP^{WT}, AHSP^{P30A}, and AHSP^{P30W}. The fitted values of $k'_{\alpha\beta}$ were in the range of 0.2–1.0 μM^{-1} s^{-1}, which are similar to the values reported for the association of deoxygenated α and β (39). The equilibrium dissociation con-

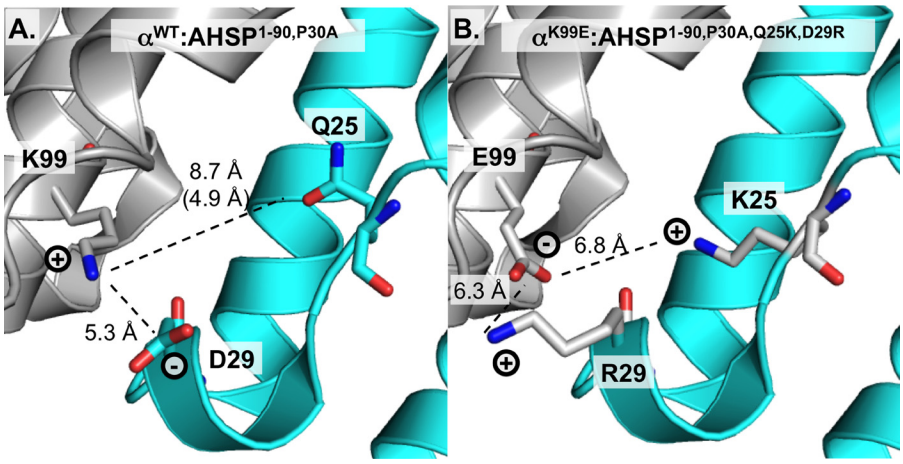

FIGURE 6. **Possible electrostatic interactions at or near Pro^{30} loop at the α-AHSP interface.** Images in both panels were generated from an x-ray crystal structure of AHSP^{P30A}(1–90) in complex with met-α (Protein Data Bank code 1Z8U (15)). *A*, possible interactions at the AHSP-α interface. The *parenthetical* distance was determined using structural data obtained from Protein Data Bank structure code 1Y01 (14). *B*, hypothetical structures for AHSP revertant mutants (Q25K and D29R) that allow binding of α^{K99E}, Hb Turriff. In both panels, the color scheme is the same as in Fig. 5. Distances were measured and the theoretical model was generated using the PyMOL Molecular Graphics System distance measuring utility and site-directed mutagenesis wizard, respectively.

stants for the corresponding α·AHSP complexes were calculated from the ratio k_{AHSP}/k'_{AHSP}.

Although k'_{AHSP} appears to be invariant, the rate of α dissociation from AHSP is strongly dependent on both the size of the amino acid at position 30 of AHSP and the oxidation state of α. For αCO^{WT}, the P30A AHSP mutation had little effect on k_{AHSP}, but the P30W mutation caused a marked 25-fold decrease in k_{AHSP} (Table 1). The value of k_{AHSP} for the reduced forms of α^{WT} is ≈0.2 s^{-1}, but the value for met-α is 100-fold lower and gives rise to a subnanomolar value for $K_{D(AHSP)}$. The time courses for met-α dissociation from AHSP^{P30A} show heterogeneity (see Table 1, footnote *c*; see Fig. 2B in Ref. 36), suggesting multiple conformations for the mutant AHSP^{P30A}·met-α complex. However, even the rate of the most rapid phase is 5–10-fold smaller than k_{AHSP} for the corresponding reduced α complex.

Effects of Other Mutations in AHSP Pro^{30} Loop and α^{K99E} Subunit Variant—Previous studies of AHSP^{WT} have revealed detailed structural information regarding the α·AHSP binding interface, including the identities of all the α chain amino acids that are thought to interact directly with AHSP (14, 15). In a previous study (40), we used this information as a basis for conducting literature-based searches for clinically significant α variants possessing mutations at these positions. It was hypothesized that the phenotypes associated with these mutations might be a result of aberrant α^{mutant}·AHSP^{WT} interactions. Using a series of indirect binding studies, eight α missense mutations were investigated, and one was found to affect the α-AHSP interface without detectably perturbing αβ subunit interactions (40). This mutation, called Hb Turriff, replaces α Lys^{99} with Glu (40).

To extend this work, we designed a series of AHSP mutants, which were hypothesized to restore binding to α^{K99E} (40). As shown in Fig. 6*A*, the α^{WT} Lys^{99} residue is positioned in close proximity to AHSP^{WT} Pro^{30} when the two proteins are bound together. The α K99E mutation is predicted to perturb this region of the α-AHSP interface by introducing a negative charge and generating unfavorable electrostatic interactions with neighboring AHSP^{WT} residues. To alter the charge on the complementary surface of AHSP^{WT} and investigate the relative importance of electrostatic interactions in this region, Gln^{25} and Asp^{29} in AHSP were mutated to Lys and Arg, respectively. Hypothetical structures showing possible side chain rotamers in the mutant AHSP proteins are shown in Fig. 6*B*.

We expressed and purified these AHSP mutant proteins along with recombinant Hb Turriff. We then isolated the individual subunits of Hb Turriff to obtain α^{K99E}. All proteins were stable and found to behave similarly to their wild-type counterparts throughout the purifications. Although α^{K99E} exhibited altered mobility during diethylaminoethyl cellulose chromatography, this protein was still resolvable from both tetrameric Hb Turriff and β. The finding that Hb Turriff was expressed at the usual levels confirms our previous work, which suggested that the K99E mutation does not significantly perturb αβ subunit interactions.

The following sets of binding and dissociation reactions were investigated using reduced αCO variants: 1) α^{K99E} binding to AHSP^{WT}, 2) α^{K99E} binding to AHSP^{Q25K}, 3) α^{K99E} binding to AHSP^{D29R}, 4) α^{WT} binding to AHSP^{Q25K}, and 5) α^{WT} binding to AHSP^{D29R}. Representative time courses as well as fits to the kinetic expressions for association ($k_{obs} = k'_{AHSP} + k_{AHSP}$) and dissociation (Equation 1) for these experiments are shown in Fig. 7, *A–D*. Longer time scales were investigated, and small slow phases with highly variable amplitudes and rates were observed for all these AHSP variants, which still have Pro at position 30. The rate and equilibrium constants for the major fast phases of these reactions are given in Table 2.

These results agree with our previous work (40) and with the data of Feng *et al.* (14), which showed that the α K99A mutation disrupts binding to AHSP^{WT}. In the case of the α K99E mutation, no binding to AHSP^{WT} was detected at all even at high micromolar concentrations of both proteins. Weak binding could be restored with the Q25K AHSP mutation, and moderate binding occurred with the D29R AHSP variant. Thus, it seems likely that the ϵ-amino group of α^{WT} Lys^{99} participates in favorable electrostatic interactions with one or more polar side

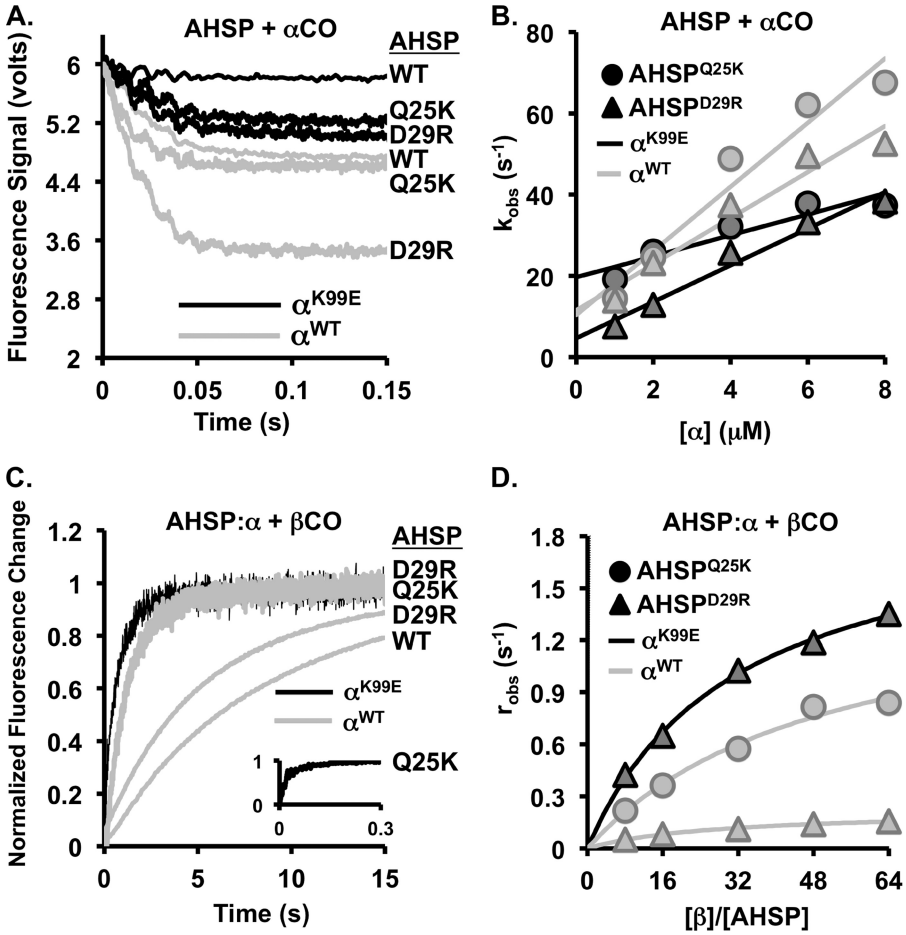

FIGURE 7. **Time courses and kinetics for α^{K99E}CO binding to AHSP revertant mutants.** *A*, time courses for α^{WT}CO and α^{K99E}CO binding to AHSP^{WT}, AHSP^{Q25K}, and AHSP^{D29R}. *B*, determination of the association rate constants (k'_{AHSP}) under pseudo-first-order for the reactions in *A*. *C*, representative replacement reaction time courses for the displacement of α^{WT}CO and α^{K99E}CO from AHSP^{WT}, AHSP^{Q25K}, and AHSP^{D29R} by βCO. *D*, dependence of the replacement rates on [βCO]/[AHSP]; *lines* represent theoretical fits to Equation 1.

TABLE 2

Rates of α^{WT} and α^{K99E} binding to and dissociation from AHSP^{Q25K} and AHSP^{D29R}

The association (k'_{AHSP}) and dissociation (k_{AHSP}) rate constants were obtained from the kinetic data in Fig. 7, and the equilibrium dissociation constants ($K_{D(AHSP)}$) were calculated from the ratio k_{AHSP}/k'_{AHSP}. The abbreviation "ND" signifies that a given value could not be determined. No binding of α^{K99E}CO to AHSP^{WT} could be detected presumably because of very large k_{AHSP} and $K_{D(AHSP)}$ values. In the case of α^{K99E} binding to AHSP^{Q25K}, we were unable to measure displacement reactions, and k_{AHSP} was calculated based on the *y*-intercept of the association reaction measured under pseudo-first-order conditions (plot in Fig. 7*B*).

Reaction	k'_{AHSP}	k_{AHSP}	$k'_{\alpha\beta}$	$K_{D(AHSP)}$
	$\mu M^{-1}\ s^{-1}$	s^{-1}	$\mu M^{-1}\ s^{-1}$	nM
AHSP^{WT} + α^{WT}	10 ± 1.9	0.17	0.26	17
AHSP^{WT} + α^{K99E}CO	ND	>1,000	ND	>10,000
AHSP^{Q25K} + α^{K99E}CO	2.5	17.5	ND	7,000
AHSP^{D29R} + α^{K99E}CO	4.5	2.0	0.14	440
AHSP^{Q25K} + α^{WT}CO	7.9	1.6	0.15	200
AHSP^{D29R} + α^{WT}CO	5.7	0.22	0.20	39

chains on AHSP^{WT}. However, because α^{WT} could still bind fairly strongly to AHSP^{Q25K} and AHSP^{D29R}, it also seems likely that the K99E α mutation causes other conformational alterations in the globin structure.

Rapid and Reversible AHSP-induced α Hemichrome Formation—HbA autooxidation is a spontaneous process in which either O_2 bound to a ferrous heme group spontaneously dissociates as a superoxide radical, or O_2 free in solution reacts with a transient aquo-deoxyheme, leaving the resulting iron in the ferric (Fe^{3+}) state (41–43). Following this reaction, the hemin iron is axially coordinated on one side by a histidine (the proximal or F8 histidine) and on the other by an H_2O or OH^- depending on pH (44, 45). If the hemin pocket unfolds, the distal histidine, His^{58}(E7) in α (or other nearby basic amino acids on the distal side of the heme ring) can coordinate to the ferric iron atom (44–48) The resulting bishistidyl adduct is called a hemichrome (44, 45). Bishistidyl adducts can also form with ferrous heme groups, and the resulting products are termed hemochromes (44, 45). These species can be identified by characteristic peaks in the visible spectra of the corresponding metHb and deoxy-Hb derivatives (44, 45).

Previous work has shown that binding to AHSP accelerates the autooxidation of αO_2 to form a hemichrome with no readily identifiable intermediate aquo-met-α state (14, 18). At neutral

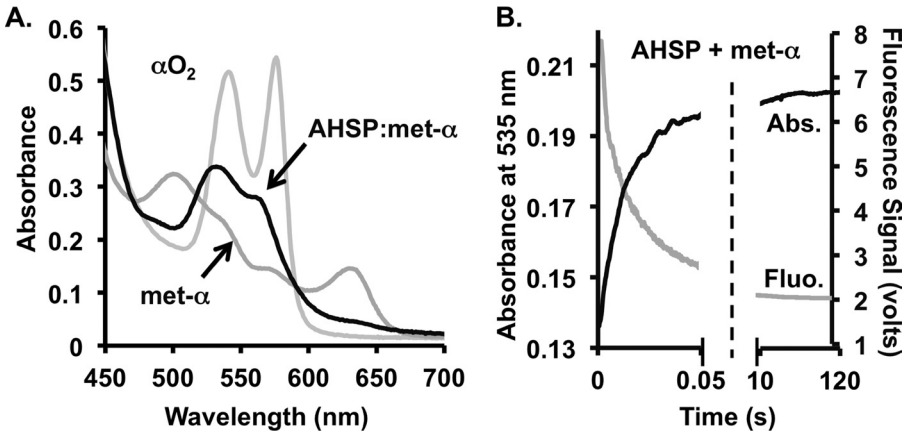

FIGURE 8. **Comparison of visible spectra of αO_2, free met-α, and met-α bound to AHSP.** *A*, optical absorbance spectra of 40 μM α^{WT} in the free O_2-bound and ferric forms and in $AHSP^{WT}$·met-α^{WT} complex. Spectra for free αO_2 and met-α were recorded before and after (1–2 min) adding a 5-fold molar excess of potassium ferricyanide. The spectrum of the $AHSP^{WT}$·met-α^{WT} complex was measured by first adding a 5-fold molar excess of potassium ferricyanide to the original αO_2 solution and then adding $AHSP^{WT}$ to the newly formed met-α. *B*, optical absorbance (535 nm) and fluorescence emission (>302 nm) time courses observed after mixing 20 μM met-α^{WT} with 20 μM $AHSP^{WT}$ in a stopped-flow rapid mixing spectrometer. met-α^{WT} was generated immediately before mixing with AHSP by adding a 5-fold excess of potassium ferricyanide to the stock syringe containing $\alpha^{WT}O_2$. The half-times for the absorbance increase due to hemichrome formation and the fluorescence decrease due to met-α binding to AHSP are the same, and the apparent bimolecular rate constants are almost identical (5–10 μM^{-1} s^{-1}) to those determined in fluorescence experiments similar to those shown in Fig. 1.

pH, rapid oxidation of free αO_2 by ferricyanide initially produces met-α with water coordinated to the sixth position of the iron atom. The spectral differences between αO_2 and met-α are shown in Fig. 8*A* with the ferrous oxygenated form exhibiting strong absorption peaks at 541 and 576 nm and aquo-met-α exhibiting large charge transfer bands peaking at ~505 and 635 nm (29, 30). Adding equimolar AHSP to met-α resulted in the immediate (≤10 s) disappearance of the 505 and 635 nm bands and appearance of 535 and 565 nm bands, which are characteristic of hemichrome formation (Fig. 8*A*) (11, 44).

The kinetics of this spectral transition are shown in Fig. 8*B*. When 20 μM met-α was mixed with 20 μM AHSP, a large increase in absorbance was observed at 535 nm. The apparent bimolecular rate is 5–10 μM^{-1} s^{-1}, which is identical to that observed when measuring binding by quenching of intrinsic AHSP fluorescence (Fig. 8*B*, *gray* time course). These results show that met-α hemichrome formation occurs simultaneously with binding to AHSP and that the conformational transition from aquo-met to the hemichrome form of α occurs at rates >100 s^{-1} when bound to AHSP. If the hemichrome conformational change were slower, it would have been seen as a much slower 535-nm absorbance increase in Fig. 8*B* compared with the AHSP fluorescence decrease.

To investigate the reversibility of AHSP-induced hemichrome formation with respect to reduction, a solution of met-α·AHSP complex was rapidly mixed with excess sodium dithionite. This reagent is a reducing agent, which both consumes O_2 in aqueous solutions and rapidly converts metHbA to ferrous deoxy-HbA (1, 30). As is shown in Fig. 9, rereduction of met-α·AHSP did not produce a spectrum indicative of a hemochrome, which would have had a moderate peak at ~530 nm and a very intense band at 558 nm (44, 49). Instead, reduction with dithionite produced a deoxy-α spectrum with a single peak at ~560 nm, which is characteristic of pentacoordinate deoxy-α in its native and fully folded form even though the subunit is still bound to AHSP (29). The time course of the reduction reaction was measured in a rapid scanning, stopped-flow spectrophotometer. The resulting time courses indicate that rereduction occurred rapidly (Fig. 9, *inset*) with an observed rate that is on the same order as the rate of reduction of free met-α (data not shown), and no hemochrome intermediates were observed. Thus, the α conformational changes after reduction are also very rapid even when the globin is bound to AHSP.

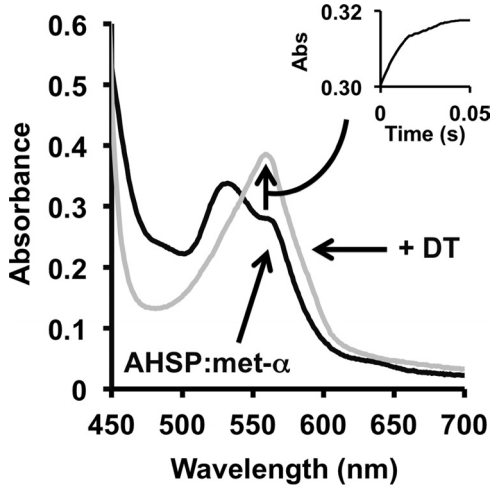

FIGURE 9. **Chemical reduction of AHSP·met-α^{WT} complexes.** Spectra were recorded before and after the addition of excess sodium dithionite (*DT*) (~15 mM) to 40 μM α^{WT}·$AHSP^{WT}$ complexes. *Inset*, emergence of the deoxy-α^{WT} absorption peak at 558 nm after mixing AHSP·met-α^{WT} with the same amount of reductant in a stopped-flow rapid mixing apparatus. Spectra were also recorded every 1 ms and analyzed (data not shown). There was no evidence for transient formation of a hemochrome intermediate.

DISCUSSION

The two phases observed for the reaction of α^{WT} with $AHSP^{WT}$ (Figs. 1 and 4) seem to verify the structural heterogeneity first characterized by Santiveri *et al.* (13). The loss of the second, slow phase for the P30A and P30W AHSP mutations (Fig. 2) suggests strongly that the kinetic heterogeneity is due to peptidylprolyl cis-trans isomerization at the Asp^{29}-Pro^{30} pep-

tide bond in AHSP. Based on the relative amplitude of the slow association phase, it appears that 20–30% of free $AHSP^{WT}$ occupies a cis peptidylprolyl conformation that is relatively unreactive toward reduced α. Although this estimate differs from the 50% mixture reported by Santiveri *et al.* (13), it is consistent with previous reports that at equilibrium 60–90% of model oligopeptides occupy the trans peptidylprolyl conformation and 10–40% occupy the cis conformation (for a review, see Ref. 50). Although more recent work has revealed that the exact ratios are dependent on which amino acid precedes Pro, in cases of Asp-Pro, it has been shown that 11–19% of model oligopeptides occupy the cis peptidyl-prolyl conformation (51). Additionally, the observed rate of the slow phase, 0.04 ± 0.01 s^{-1} in 100 mM potassium phosphate buffer at pH 7.4 at 22 °C, is consistent both with the rate assignment of AHSP conformational interconversion by NMR (13) and with other studies that show that peptidylprolyl cis-trans interconversions occur spontaneously with half-times of 10–100 s at 25 °C (50). The observations that the rate of the slow phase was independent of α concentration and that the slow phase was not observed when α was limiting are also supportive of this model. This mechanism implies that reduced α reacts rapidly with the trans Pro^{30} conformer of AHSP in a simple bimolecular process (Reaction 1), whereas little or no binding occurs to the small remaining fraction of cis AHSP until it isomerizes to the trans conformation.

This interpretation is supported by the effects of the P30A and P30W AHSP mutations, which caused the formation of a single trans conformation at the 29-30 peptide bond (Fig. 3) (13). The time courses for α binding to $AHSP^{P30A}$ and $AHSP^{P30W}$ are monophasic and bimolecular. The fitted values of k'_{AHSP} for these mutants are almost identical to that obtained from the fast phase for α binding to $AHSP^{WT}$. This finding also suggests strongly that reduced α binds rapidly to the trans peptidylprolyl Pro^{30} conformer of $AHSP^{WT}$. This idea is supported by the observation that the wild-type α·AHSP complex was very difficult to crystallize, and formation of crystals was greatly facilitated by the P30A mutation (14–16).

However, none of these arguments for cis to trans peptidylprolyl isomerization are direct, and we did not observe an effect on the amplitude or rate of the slow phase when peptidylprolyl isomerases were added to the AHSP solution prior to mixing with α. Thus, it is possible that the slow phases observed for $AHSP^{WT}$ reflect some other type of conformational isomerization that causes more quenching of intrinsic AHSP fluorescence after reduced α is bound. Some autooxidation is occurring when αO_2 is bound, but the AHSP·αCO complex is stable with little or no UV-visible absorbance changes occurring on time scales of minutes to hours. The lack of a slow phase for met-α binding to $AHSP^{WT}$ suggests that the rapidly formed α hemichrome binds to either prolyl conformer.

The importance of the loop separating helices 1 and 2 of $AHSP^{WT}$ is underscored by our studies of α^{K99E} (Hb Turriff). Our preliminary studies indicated that this variant is unstable *in vivo* due to a loss of binding to $AHSP^{WT}$ (40). Our new studies confirm that this mutant α cannot bind AHSP even at micromolar concentrations and that the mild phenotype associated with Hb Turriff is caused by a loss of this interaction and not by disrupted assembly into αβ dimers and tetramers, which appears normal.

The results in Table 2 show that introduction of positively charge amino acids in the Pro^{30} loop of AHSP revertants can partially reverse the effects of the α K99E mutation. However, the results are complex and indicate that, although favorable electrostatic interactions are important near the Pro^{30} loop, other conformational factors also play an important role.

The association and dissociation rate constants reported for αCO and αO_2 binding to AHSP in Table 1 agree well with those in our initial report (19) and with the parameters reported subsequently by Brillet *et al.* (35). However, Brillet *et al.* (35) reported that the "… dissociation rates were not found to depend strongly on the Hb oxidation state (oxy *versus* met *versus* deoxy)." Although our data also show that k'_{AHSP} is nearly the same for ferric and ferrous α (Table 1), the rate of dissociation (k_{AHSP}) of the met-α·$AHSP^{WT}$ complex is ~100-fold smaller than that for the reduced α·AHSP complexes. The net result is a 100-fold higher affinity and a very small subnanomolar K_D for met-α binding to AHSP.

Gell *et al.* (16) observed a similar large relative decrease in K_D for met-α *versus* αCO binding to AHSP using isothermal titration calorimetry (Table 1). However, the absolute K_D values obtained by calorimetry are consistently higher than either we or Brillet *et al.* (35) determined from the ratio of the kinetic parameters. The reasons for this discrepancy are not obvious. The cause may be related to systematic errors during curve fitting that arise because of the high concentrations of protein (1–5 μM) required by the isothermal titration calorimetry experiments and the low K_D values (≤0.1 μM; Table 1).

Regardless of oxidation state or bound ligand, the bimolecular rate of α binding to AHSP ($k'_{AHSP} \approx 10\ \mu M^{-1}\ s^{-1}$) is ~20-fold greater than the rate constant for α binding to β ($k'_{\alpha\beta} \approx 0.5\ \mu M^{-1}\ s^{-1}$ (Table 1 and Refs. 8, 37, 39, and 52–55)). However, the rate of α dissociation from AHSP ($k_{AHSP} \approx 0.2\ s^{-1}$ for ferrous α) is roughly 200,000-fold greater than the rate of α dissociation from αβ dimers ($k_{\alpha\beta} \approx 0.000001\ s^{-1}$ (52–54)). These findings led us to propose the model in Fig. 10 for facilitation of Hb assembly by AHSP (19).

Because AHSP binds to α more rapidly than β, it is likely that AHSP out-competes β kinetically for nascent free α *in vivo*. If the α heme groups are in the ferrous form, they can be more readily displaced by β due to their dramatically higher affinity for β chains ($K_D \approx 0.001$ nM (37, 52–54)) than for AHSP ($K_D \approx 17$ nM (Table 1)) and the relatively high rate of ferrous α·AHSP dissociation ($k_{AHSP} \approx 0.2\ s^{-1}$). However, if bound α is in the oxidized hemichrome form, displacement by β chains is 100-fold slower. Thus, participation of ferric α^{WT} in HbA assembly is inhibited kinetically by AHSP, but disassembly of the resultant met-α·AHSP complex is facilitated by hemin reduction.

Hemoglobin assembly requires apoglobin synthesis, partial folding, heme uptake, reduction, and αβ dimer formation. Although folding and assembly can occur without AHSP binding, we suggest that the highlighted pathway in Fig. 10 is favored in the presence of AHSP. AHSP first assists the folding of apo-α (17) and then uptake of hemin to generate the met-α·AHSP hemichrome complex. It has been shown that hemichrome forms are highly populated intermediates during the folding of

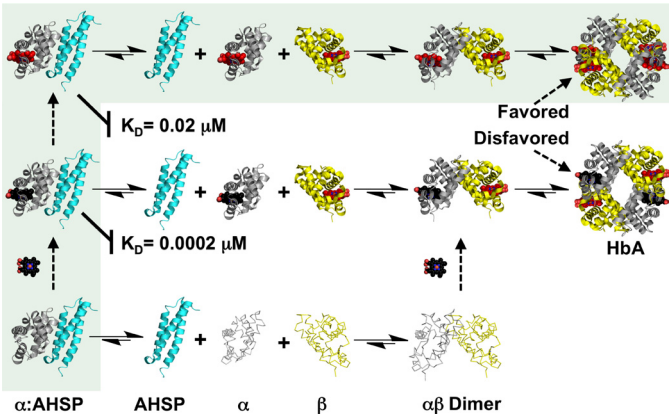

FIGURE 10. **Rates of α^{WT} binding to and dissociation from AHSP^{WT} suggest parallel chaperoned pathway for HbA assembly.** The colors for AHSP, α, and β are the same as in Fig. 5*A* except *red spheres* are used to represent ferrous heme group atoms and *black spheres* are used to represent ferric hemin atoms. AHSP, α, and β structures were generated using Protein Data Bank codes 1Z8U and 1LFL, respectively (15, 68). The highlighted pathway for α folding, hemin uptake, and incorporation into HbA was based on the following observations. Zhou *et al.* (18) have shown that reduction of met-α^{WT}·AHSP^{WT} complexes to the ferrous state is rapidly catalyzed by reductases. Binding to AHSP^{WT} facilitates heme-free apo-α folding (17, 61, 63, 64). Reduced α is readily taken up from AHSP by β, whereas met-α is kinetically trapped in the complex (Fig. 5*C*).

both holomyoglobin and holo-Hb (46–48). The α hemichrome folding intermediate is unstable when free in solution, loses hemin, and unfolds rapidly in the apoform, leading to precipitation (44–48). However, this met-α folding intermediate is stabilized by AHSP. When the met-α·AHSP complex is reduced, fully folded reduced deoxy- or αO_2 is formed, has a lower affinity for AHSP, and is rapidly displaced by β.

Free αO_2 monomers are reportedly more prone to autooxidation than βO_2 (56) and are produced in a slight excess during normal HbA production *in vivo* probably to compensate for this instability (for a review, see Ref. 19). In general, ferric subunits and metHbA are much less stable than their ferrous forms due to enhanced rates of hemin loss and subsequent rapid apoprotein denaturation (57–65). Our data and the scheme in Fig. 10 suggest that AHSP^{WT} promotes the formation of more stable HbA end products by acting as a quality control checkpoint during the assembly process. The relative importance of this function is likely amplified during periods of oxidative stress or during the spontaneous accumulation of ferric α^{WT}. Instead of these subunits reacting directly with β to form relatively unstable, partially oxidized HbA tetramers, ferric α chains are sequestered kinetically in AHSP complexes until the iron can be reduced.

This redox proofreading function and stabilization of the hemichrome folding intermediate helps explain the findings of Khandros *et al.* (36) that demonstrate that Pro^{30} substitutions (P30W and P30A) do not appear to significantly affect HbA production or AHSP function *in vivo*. The P30W mutation enhances the affinity of AHSP for αO_2 and slows its autooxidation rate, but these properties appear to be less important than high affinity binding to met-α chains. These *in vivo* data also suggest that cis-trans peptidylprolyl isomerization in AHSP^{WT} is not critical physiologically because only the trans conformation occurs in the Pro^{30} mutants, which have no obvious phenotype. The key biochemical property of AHSP appears to be its high affinity for oxidized α.

The mechanism in Fig. 10 shows why the lack of K99E α binding to AHSP indirectly destabilizes HbA. When this variant is oxidized, it cannot be sequestered by AHSP, which allows ferric α^{K99E} to either denature or react with β and be incorporated into relatively unstable mixed valency tetramers. Both the stabilization and quality control functions help explain the observation that disruption of AHSP^{WT} in mice worsens the phenotypes of both α- and β-thalassemia syndromes (66, 67).

Although HbA assembly almost certainly occurs through several parallel pathways, AHSP binding appears to act as a shunt for ferric α until reduction can occur. Thus, even when β subunits are in excess (α-thalassemia), there will be more incorporation of unstable oxidized α into HbA when AHSP is absent, leading to more globin precipitates. In the case of excess α (β-thalassemia), the situation is even worse in the absence of AHSP when no chaperone is available to stabilize the excess met-α.

CONCLUSIONS

Cis-trans isomerization and electrostatic interactions in the Pro^{30} loop between helices 1 and 2 of AHSP have marked effects on the rate and equilibrium constants for α binding and can help explain the phenotypes of α hemoglobinopathies that involve disruption of α binding to AHSP but not to β. Compared with ferrous α, met-α binds 100-fold more tightly to AHSP, resulting in a very low rate of dissociation of the ferric α·AHSP complex. Consequently, AHSP can trap met-α kinetically and inhibit its incorporation into unstable mixed valence HbA tetramers. This kinetic property coupled with AHSP stabilization of the hemichrome folding intermediate supports a dual role for AHSP. It acts both as a molecular chaperone to facilitate α folding and as a quality control protein to prevent assembly of unstable, partially oxidized Hb tetramers.

Acknowledgments—We thank Eileen W. Singleton and Jayashree Soman for assistance preparing Hb Turriff.

REFERENCES

1. Bunn, H. F., and Forget, B. G. (1986) *Hemoglobin: Molecular, Genetic and Clinical Aspects*, W. B. Saunders Co., Philadelphia
2. Schechter, A. N. (2008) Hemoglobin research and the origins of molecular medicine. *Blood* **112,** 3927–3938
3. Steinberg, M. H. (2001) *Disorders of Hemoglobin: Genetics, Pathophysiology, and Clinical Management*, Cambridge University Press, Cambridge, UK
4. Weatherall, D. J. (1998) Pathophysiology of thalassaemia. *Baillieres Clin. Haematol.* **11,** 127–146
5. Benz, E. J., Jr., and Forget, B. G. (1974) The biosynthesis of hemoglobin. *Semin. Hematol.* **11,** 463–523
6. Antonini, E., and Chiancone, E. (1977) Assembly of multisubunit respiratory proteins. *Annu. Rev. Biophys. Bioeng.* **6,** 239–271
7. Friedman, F. K., and Beychok, S. (1979) Probes of subunit assembly and reconstitution pathways in multisubunit proteins. *Annu. Rev. Biochem.* **48,** 217–250
8. Bunn, H. F. (1987) Subunit assembly of hemoglobin: an important determinant of hematologic phenotype. *Blood* **69,** 1–6
9. Voon, H. P., and Vadolas, J. (2008) Controlling α-globin: a review of α-glo-

bin expression and its impact on β-thalassemia. *Haematologica* **93,** 1868–1876
10. Perutz, M. F., Rossmann, M. G., Cullis, A. F., Muirhead, H., Will, G., and North, A. C. (1960) Structure of haemoglobin: a three-dimensional Fourier synthesis at 5.5-Å resolution, obtained by x-ray analysis. *Nature* **185,** 416–422
11. Kihm, A. J., Kong, Y., Hong, W., Russell, J. E., Rouda, S., Adachi, K., Simon, M. C., Blobel, G. A., and Weiss, M. J. (2002) An abundant erythroid protein that stabilizes free α-haemoglobin. *Nature* **417,** 758–763
12. Gell, D., Kong, Y., Eaton, S. A., Weiss, M. J., and Mackay, J. P. (2002) Biophysical characterization of the α-globin binding protein α-hemoglobin stabilizing protein. *J. Biol. Chem.* **277,** 40602–40609
13. Santiveri, C. M., Pérez-Cañadillas, J. M., Vadivelu, M. K., Allen, M. D., Rutherford, T. J., Watkins, N. A., and Bycroft, M. (2004) NMR structure of the α-hemoglobin stabilizing protein: insights into conformational heterogeneity and binding. *J. Biol. Chem.* **279,** 34963–34970
14. Feng, L., Gell, D. A., Zhou, S., Gu, L., Kong, Y., Li, J., Hu, M., Yan, N., Lee, C., Rich, A. M., Armstrong, R. S., Lay, P. A., Gow, A. J., Weiss, M. J., Mackay, J. P., and Shi, Y. (2004) Molecular mechanism of AHSP-mediated stabilization of α-hemoglobin. *Cell* **119,** 629–640
15. Feng, L., Zhou, S., Gu, L., Gell, D. A., Mackay, J. P., Weiss, M. J., Gow, A. J., and Shi, Y. (2005) Structure of oxidized α-haemoglobin bound to AHSP reveals a protective mechanism for haem. *Nature* **435,** 697–701
16. Gell, D. A., Feng, L., Zhou, S., Jeffrey, P. D., Bendak, K., Gow, A., Weiss, M. J., Shi, Y., and Mackay, J. P. (2009) A cis-proline in α-hemoglobin stabilizing protein directs the structural reorganization of α-hemoglobin. *J. Biol. Chem.* **284,** 29462–29469
17. Krishna Kumar, K., Dickson, C. F., Weiss, M. J., Mackay, J. P., and Gell, D. A. (2010) AHSP (α-haemoglobin-stabilizing protein) stabilizes apo-α-haemoglobin in a partially folded state. *Biochem. J.* **432,** 275–282
18. Zhou, S., Olson, J. S., Fabian, M., Weiss, M. J., and Gow, A. J. (2006) Biochemical fates of α hemoglobin bound to α hemoglobin-stabilizing protein AHSP. *J. Biol. Chem.* **281,** 32611–32618
19. Mollan, T. L., Yu, X., Weiss, M. J., and Olson, J. S. (2010) The role of α-hemoglobin stabilizing protein in redox chemistry, denaturation, and hemoglobin assembly. *Antioxid. Redox Signal.* **12,** 219–231
20. Weiss, M. J., and dos Santos, C. O. (2009) Chaperoning erythropoiesis. *Blood* **113,** 2136–2144
21. Weiss, M. J., Zhou, S., Feng, L., Gell, D. A., Mackay, J. P., Shi, Y., and Gow, A. J. (2005) Role of α-hemoglobin-stabilizing protein in normal erythropoiesis and β-thalassemia. *Ann. N.Y. Acad. Sci.* **1054,** 103–117
22. Shen, T. J., Ho, N. T., Zou, M., Sun, D. P., Cottam, P. F., Simplaceanu, V., Tam, M. F., Bell, D. A., Jr., and Ho, C. (1997) Production of human normal adult and fetal hemoglobins in *Escherichia coli*. *Protein Eng.* **10,** 1085–1097
23. Birukou, I., Schweers, R. L., and Olson, J. S. (2010) Distal histidine stabilizes bound O_2 and acts as a gate for ligand entry in both subunits of adult human hemoglobin. *J. Biol. Chem.* **285,** 8840–8854
24. Wiedermann, B. L., and Olson, J. S. (1975) Acceleration of tetramer formation by the binding of inositol hexaphosphate to hemoglobin dimers. *J. Biol. Chem.* **250,** 5273–5275
25. Geraci, G., Parkhurst, L. J., and Gibson, Q. H. (1969) Preparation and properties of α- and β-chains from human hemoglobin. *J. Biol. Chem.* **244,** 4664–4667
26. Bucci, E., and Fronticelli, C. (1965) A new method for the preparation of α and β subunits of human hemoglobin. *J. Biol. Chem.* **240,** PC551–PC552
27. Boyer, P. D. (1954) Spectrophotometric study of protein sulfhydryl groups with organic mercurials. *J. Am. Chem. Soc.* **76,** 4331–4337
28. Mollan, T. L. (2011) *The Role of Alpha-Hemoglobin Stabilizing Protein in Hemoglobin Subunit Assembly*. Ph.D. Thesis, Rice University
29. Banerjee, R., Alpert, Y., Leterrier, F., and Williams, R. J. (1969) Visible absorption and electron spin resonance spectra of the isolated chains of human hemoglobin. Discussion of chain-mediated heme-heme interaction. *Biochemistry* **8,** 2862–2867
30. Antonini, E., and Brunori, M. (1971) *Hemoglobin and Myoglobin in Their Reactions with Ligands*, pp. 13–54, Elsevier, Amsterdam
31. Kemmer, G., and Keller, S. (2010) Nonlinear least-squares data fitting in Excel spreadsheets. *Nat. Protoc.* **5,** 267–281
32. Baudin-Creuza, V., Vasseur-Godbillon, C., Pato, C., Préhu, C., Wajcman, H., and Marden, M. C. (2004) Transfer of human α- to β-hemoglobin via its chaperone protein: evidence for a new state. *J. Biol. Chem.* **279,** 36530–36533
33. Alpert, B., Jameson, D. M., and Weber, G. (1980) Tryptophan emission from human hemoglobin and its isolated subunits. *Photochem. Photobiol.* **31,** 1–4
34. Leutzinger, Y., and Beychok, S. (1981) Kinetics and mechanism of heme-induced refolding of human α-globin. *Proc. Natl. Acad. Sci. U.S.A.* **78,** 780–784
35. Brillet, T., Baudin-Creuza, V., Vasseur, C., Domingues-Hamdi, E., Kiger, L., Wajcman, H., Pissard, S., and Marden, M. C. (2010) α-Hemoglobin stabilizing protein (AHSP), a kinetic scheme of the action of a human mutant, AHSPV56G. *J. Biol. Chem.* **285,** 17986–17992
36. Khandros, E., Mollan, T. L., Yu, X., Wang, X., Yao, Y., D'Souza, J., Gell, D. A., Olson, J. S., and Weiss, M. J. (2012) Insights into hemoglobin assembly through *in vivo* mutagenesis of α-hemoglobin stabilizing protein. *J. Biol. Chem.* **287,** 11325–11337
37. Shaeffer, J. R., McDonald, M. J., Turci, S. M., Dinda, D. M., and Bunn, H. F. (1984) Dimer-monomer dissociation of human hemoglobin A. *J. Biol. Chem.* **259,** 14544–14547
38. Rohlfs, R. J., Mathews, A. J., Carver, T. E., Olson, J. S., Springer, B. A., Egeberg, K. D., and Sligar, S. G. (1990) The effects of amino acid substitution at position E7 (residue 64) on the kinetics of ligand binding to sperm whale myoglobin. *J. Biol. Chem.* **265,** 3168–3176
39. McGovern, P., Reisberg, P., and Olson, J. S. (1976) Aggregation of deoxyhemoglobin subunits. *J. Biol. Chem.* **251,** 7871–7879
40. Yu, X., Mollan, T. L., Butler, A., Gow, A. J., Olson, J. S., and Weiss, M. J. (2009) Analysis of human α globin gene mutations that impair binding to the α hemoglobin stabilizing protein. *Blood* **113,** 5961–5969
41. Brantley, R. E., Jr., Smerdon, S. J., Wilkinson, A. J., Singleton, E. W., and Olson, J. S. (1993) The mechanism of autooxidation of myoglobin. *J. Biol. Chem.* **268,** 6995–7010
42. Rifkind, J. M., Ramasamy, S., Manoharan, P. T., Nagababu, E., and Mohanty, J. G. (2004) Redox reactions of hemoglobin. *Antioxid. Redox Signal.* **6,** 657–666
43. Brunori, M., Falcioni, G., Fioretti, E., Giardina, B., and Rotilio, G. (1975) Formation of superoxide in the autoxidation of the isolated α and β chains of human hemoglobin and its involvement in hemichrome precipitation. *Eur. J. Biochem.* **53,** 99–104
44. Rifkind, J. M., Abugo, O., Levy, A., and Heim, J. (1994) Detection, formation, and relevance of hemichromes and hemochromes. *Methods Enzymol.* **231,** 449–480
45. Vergara, A., Vitagliano, L., Verde, C., di Prisco, G., and Mazzarella, L. (2008) Spectroscopic and crystallographic characterization of bis-histidyl adducts in tetrameric hemoglobins. *Methods Enzymol.* **436,** 425–444
46. Culbertson, D. S. (2010) *Role of Heme in the Folding and Assembly of Globins*. Ph.D. Thesis, Rice University
47. Culbertson, D. S., and Olson, J. S. (2010) Role of heme in the unfolding and assembly of myoglobin. *Biochemistry* **49,** 6052–6063
48. Gomes, C. M., and Wittung-Stafshede, P. (2011) *Protein Folding and Metal Ions: Mechanisms, Biology and Disease*, pp. 97–124, CRC Press, Boca Raton, FL
49. Rachmilewitz, E. A., Peisach, J., and Blumberg, W. E. (1971) Studies on the stability of oxyhemoglobin A and its constituent chains and their derivatives. *J. Biol. Chem.* **246,** 3356–3366
50. Schmid, F. X. (1993) Prolyl isomerase: enzymatic catalysis of slow protein-folding reactions. *Annu. Rev. Biophys. Biomol. Struct.* **22,** 123–142
51. Zoldák, G., Aumüller, T., Lücke, C., Hritz, J., Oostenbrink, C., Fischer, G., and Schmid, F. X. (2009) A library of fluorescent peptides for exploring the substrate specificities of prolyl isomerases. *Biochemistry* **48,** 10423–10436
52. McDonald, M. J., Turci, S. M., Mrabet, N. T., Himelstein, B. P., and Bunn, H. F. (1987) The kinetics of assembly of normal and variant human oxyhemoglobins. *J. Biol. Chem.* **262,** 5951–5956
53. Mrabet, N. T., McDonald, M. J., Turci, S., Sarkar, R., Szabo, A., and Bunn, H. F. (1986) Electrostatic attraction governs the dimer assembly of human hemoglobin. *J. Biol. Chem.* **261,** 5222–5228
54. Mrabet, N. T., Shaeffer, J. R., McDonald, M. J., and Bunn, H. F. (1986)

Dissociation of dimers of human hemoglobins A and F into monomers. *J. Biol. Chem.* **261,** 1111–1115
55. Kawamura, Y., and Nakamura, S. (1983) Assembly of oxyhemoglobin from isolated α and β chains. *J. Biochem.* **93,** 1159–1166
56. Mansouri, A., and Winterhalter, K. (1973) Nonequivalence of chains in hemoglobin oxidation. *Biochemistry* **12,** 4946–4949
57. Yip, Y. K., Waks, M., and Beychok, S. (1977) Reconstitution of native human hemoglobin from separated globin chains and alloplex intermediates. *Proc. Natl. Acad. Sci. U.S.A.* **74,** 64–68
58. Yip, Y. K., Waks, M., and Beychok, S. (1972) Influence of prosthetic groups on protein folding and subunit assembly. I. Conformational differences between separated human α- and β-globins. *J. Biol. Chem.* **247,** 7237–7244
59. Waks, M., Yip, Y. K., and Beychok, S. (1973) Influence of prosthetic groups on protein folding and subunit assembly. Recombination of separated human α-and β-globin chains with heme and alloplex interactions of globin chains with heme-containing subunits. *J. Biol. Chem.* **248,** 6462–6470
60. Hargrove, M. S., Whitaker, T., Olson, J. S., Vali, R. J., and Mathews, A. J. (1997) Quaternary structure regulates hemin dissociation from human hemoglobin. *J. Biol. Chem.* **272,** 17385–17389
61. Hargrove, M. S., Wilkinson, A. J., and Olson, J. S. (1996) Structural factors governing hemin dissociation from metmyoglobin. *Biochemistry* **35,** 11300–11309
62. Hargrove, M. S., Singleton, E. W., Quillin, M. L., Ortiz, L. A., Phillips, G. N., Jr., Olson, J. S., and Mathews, A. J. (1994) His^{64}(E7) → Tyr apomyoglobin as a reagent for measuring rates of hemin dissociation. *J. Biol. Chem.* **269,** 4207–4214
63. Hargrove, M. S., and Olson, J. S. (1996) The stability of holomyoglobin is determined by heme affinity. *Biochemistry* **35,** 11310–11318
64. Hargrove, M. S., Barrick, D., and Olson, J. S. (1996) The association rate constant for heme binding to globin is independent of protein structure. *Biochemistry* **35,** 11293–11299
65. Bunn, H. F., and Jandl, J. H. (1966) Exchange of heme among hemoglobin molecules. *Proc. Natl. Acad. Sci. U.S.A.* **56,** 974–978
66. Yu, X., Kong, Y., Dore, L. C., Abdulmalik, O., Katein, A. M., Zhou, S., Choi, J. K., Gell, D., Mackay, J. P., Gow, A. J., and Weiss, M. J. (2007) An erythroid chaperone that facilitates folding of α-globin subunits for hemoglobin synthesis. *J. Clin. Investig.* **117,** 1856–1865
67. Kong, Y., Zhou, S., Kihm, A. J., Katein, A. M., Yu, X., Gell, D. A., Mackay, J. P., Adachi, K., Foster-Brown, L., Louden, C. S., Gow, A. J., and Weiss, M. J. (2004) Loss of α-hemoglobin-stabilizing protein impairs erythropoiesis and exacerbates β-thalassemia. *J. Clin. Investig.* **114,** 1457–1466
68. Biswal, B. K., and Vijayan, M. (2002) Structures of human oxy- and deoxyhaemoglobin at different levels of humidity: variability in the T state. *Acta Crystallogr. D Biol. Crystallogr.* **58,** 1155–1161
69. Paoli, M., Liddington, R., Tame, J., Wilkinson, A., and Dodson, G. (1996) Crystal structure of T state haemoglobin with oxygen bound at all four haems. *J. Mol. Biol.* **256,** 775–792
70. Valdes, R., Jr., and Ackers, G. K. (1978) Self-association of hemoglobin βSH chains is linked to oxygenation. *Proc. Natl. Acad. Sci. U.S.A.* **75,** 311–314